Journal of Materials Chemistry A

Accepted Manuscript

ROYAL SOCIETY OF CHEMISTRY

www.rsc.org/materialsA

ARTICLE Journal Name

Perylenediimides as Non-Fullerene Acceptors in Bulk-Heterojunction Solar Cells (BHJSCs)

Fernando Fernández-Lázaro,*[,a] Nathalie Zink-Lorre,[a] and Ángela Sastre-Santos*[,a]

Cite this: DOI: 10.1039/x0xx00000x

Received 00th January 2012,
Accepted 00th January 2012

DOI: 10.1039/x0xx00000x

www.rsc.org/

Perylenediimides are ideal candidates for the substitution of fullerene derivatives as electron acceptors in bulk heterojunction organic solar cells due to their extremely intense light absorbance, high electron mobility and excellent photochemical stability. In this review article, we briefly highlight the recent progress in highly efficient perylenediimide dyes characterized by a reduction of the cofacial stacking without an adverse impact in their charge-transport properties, which has led to PCEs higher than 8.4%.

1. INTRODUCTION

Bulk heterojunction (BHJ) solar cells are a type of organic photovoltaic (OPV) cells that have attracted considerable attention due to some advantages, such as low cost, light weight, solution processability, fabrication on flexible substrates and large area fabrication, as well as potential for roll-to-roll production.[1] Nowadays, power conversion efficiencies (PCEs) exceeding 10% have been achieved for BHJ OPV cells based on blends of narrow bandgap polymer donors and fullerene acceptors.[2] The exploration for novel electron acceptor molecules is less developed than the search for new electron donor materials. Fullerenes and their derivatives, especially $PC_{61}BM$ and $PC_{71}BM$, have been the dominant electron acceptors in BHJ OPVs[3] because of their high electron affinity and electron mobility, isotropy of charge transport, and good ability to form favorable nanoscale networks with donor materials. However, the performances will reach a limit due to the intrinsic drawbacks and limitations of fullerenes, *e.g.* poor photostability in air, poor solar energy harvesting, difficulty in synthesis and purification, high production cost (especially for $PC_{71}BM$)[4] and the difficulty to tune the optical properties and electronic structures of fullerenes over a wide range of energy.[5] As a consequence, there is growing interest in the synthesis of non-fullerene electron acceptors for OPV,[6] which possess a strong absorption ability in the visible and NIR regions in a complementary zone to that of the electron donor, adjustable energy levels, tunable electronic properties, effective charge separation and transporting, and good match capability with donor materials.

1.1 Perylenediimides

Among all the families of electron-accepting molecules, perylenediimides (PDIs)[7] are in a prominent position due to the large number of outstanding properties they display. In particular, they possess high thermal, chemical and photochemical stabilities, the latter being an important requisite for a component in an OPV cell. PDIs absorb light intensely in the visible region. They have a strong electron-acceptor character, comparable in some cases to that of fullerene derivatives, showing also high electron mobility. Moreover, the easy functionalization of the aromatic core and imide positions allows the rational fine tuning of their solubility and HOMO-LUMO levels, as well as of the optoelectronic and self-assembling properties.[8] Finally, they are economical starting materials.

PDIs, indeed, have been used as acceptors in OPV cells, reaching three years ago PCEs of 3% (Figure 1).[9]

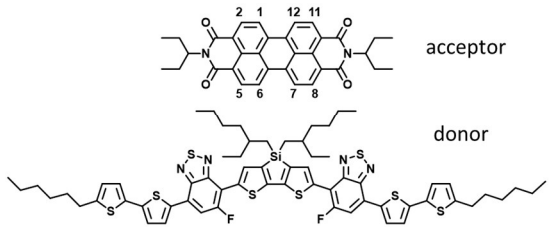

Fig. 1. p-DTS(FBTTh$_2$)$_2$:PDI BHJ OPV devices. PCE = 3.0%[9c]

However, despite these favorable properties, the evolution of the performance of PDI derivatives has not been very promising until recently. The main drawback of these molecules is the strong tendency to π-π stacking due to its planar nature, which leads to a poor solubility in most solvents and to the formation of large aggregates (typically micrometer scale) which are deleterious for the efficiency of the OPV as these aggregates allow strong self-trapping of excitons, severely limiting the exciton diffusion/separation process, which may be related to cell's relatively low fill factor (FF) and reduced short-circuit current density (J_{sc}). To solve this problem, various alkyl chains were introduced on the bay positions (positions 1, 6, 7 and 12, Figure 1) of the PDI, although performances of the corresponding OPV cells did not improve much.

At this stage, some groups initialized molecular engineering aiming at weakening the strong aggregation of PDI derivatives to avoid large crystalline aggregate domains without compromising their charge transport properties. Thus, very recently, the introduction of the ''twisted'' concept in the PDI system to diminish the aggregation has been investigated and twisted PDI compounds have been designed, mainly by means of PDI dimers linked at the imide positions or bay positions either by direct attachment or through small rings.[10] Very

promising results have been achieved with these PDI-based systems, reaching PCEs higher than 8%.
In this review, we will review the last advances in the design of perylenediimides as electron acceptor for OPV, together with some new developments in film processing of PDI-based cells.

2. Twisted PDI dimers

The three-dimensional molecular structure is a crucial factor affecting many molecular and bulk properties of the PDIs such as the electron delocalization and the electronic structures, the intra- and intermolecular interactions (hydrogen bonding, the abovementioned π–π stacking, etc.), the molecular packing in the solid (and the crystalline or amorphous nature of the latter), the solubility and processability, and the charge transport properties. Therefore, some groups have directed their research to the modification of the 3D structure of PDIs.[4]

2.1. Dimerization through rings in the bay positions

One of the pioneering works in the area compared the performances of six PDI dimers, named as **PDI 1-6**, bearing different arylene linkers, namely *p*-phenylene, *m*-phenylene, thiophene-2,5-diyl, 2,2'-bithiophene-5,5'-diyl, spirobifluorene-2,2'-diyl and spirobifluorene-2,7-diyl (Figure 2). It was expected that the linker groups should assume non-coplanar orientations with respect to the PDI units. In accordance with this presumption, the LUMOs of all dimers were maintained at a similar level to that of a PDI monomer, reassuring for adequate open-circuit voltage (V_{oc}) of solar cells. When mixed with P3HT (1-1 w/w) and introduced in a cell with an inverted configuration (ITO/ZnO/**P3HT**:acceptor/MoO_3/Ag), these PDIs yielded PCEs ranging from 0.90 to 2.35. **PDI 6**, with the spirobifluorene-2,7-diyl linker, showed the best result, with V_{oc} of 0.61 V, J_{sc} of 5.92 mA cm^{-2}, FF of 0.65 and PCE of 2.35%. **PDI 5**, with the spirobifluorene-2,2'-diyl moiety, displayed a somewhat higher J_{sc}, but worse FF and PCE than **PDI 6**.[11]

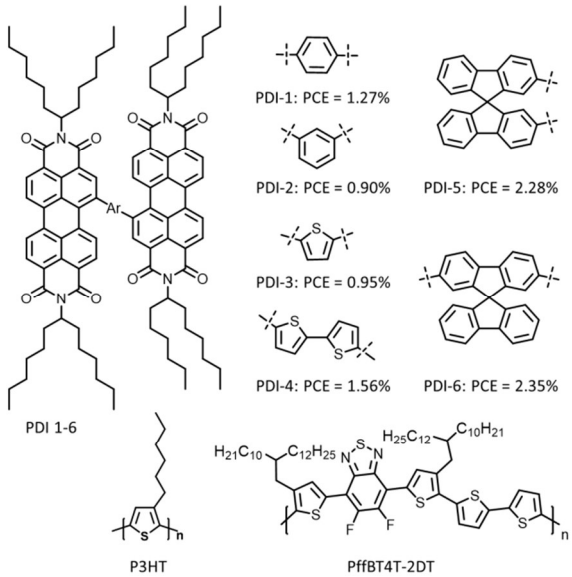

Fig. 2. Chemical structures of the PDI dimers **PDI 1-6** and the donor polymers **P3HT** and **PffBT4T-2DT**.

Later studies on **PDI 6** (named in the paper as **SF-PDI$_2$**) were conducted to find a better matching donor polymer. The best partner found was **PffBT4T-2DT** (Figure 2), taking advantage of the difluorination of the benzothiadiazole unit, which not only increases the crystallinity and hole transport ability of the polymer, but also lowers the HOMO level of the polymer, and thus increases the V_{oc} of the OPV cell. Introducing the donor and acceptor materials in an inverted structure BHJ OPV (ITO/ZnO/**PffBT4T-2DT**:**PDI 6**/V_2O_5/Al) an impressive efficiency of 6.3 was obtained (V_{oc} of 0.98 V, J_{sc} of 10.7 mA cm^{-2} and FF of 0.57). This high performance was achieved without using any additives or interlayers, which would simplify the processing and optimizations of OPV cells. The high V_{oc} was attributed to the high-lying LUMO level of **PDI 6** (because of the spirobifluorene bridge) compared to the HOMO level of **PffBT4T-2DT**. Another factor for this PCE is the reduced intermolecular aggregation (also caused by the bulky spirobifluorene bridge), which allows **PDI 6** to form films without any excessive crystallization, but keeping a reasonably good electron transport ability.[12]
Another pioneering work in this line was brought about with **Bis-PDI-T-EG** (Figure 3), a thiophene-linked PDI dimer (actually, a mixture of the three possible regioisomers). Molecular modeling indicated that the PDI dimer had a highly twisted dimeric backbone, with dihedral angles between the PDI-thienyl-PDI planes of 50°–65°, thus inducing a significant reduction in aggregation compared with the reference monomer **PDI-1**. Compared to that of **PDI-1**, the LUMO of **Bis-PDI-T-EG** was slightly depressed, by −0.10 eV, while its HOMO was considerably raised, by +0.33 eV, yielding a narrower bandgap. In order to prepare OPVs, the conjugated polymer **PBDTTT-C-T** (Figure 3) was selected as the donor material because it complemented the absorption spectrum of the PDI dimer, while the generally used **P3HT** (Figure 2) overlapped with the absorption band of the PDIs. Using the conventional architecture ITO/PEDOT:PSS/**Bis-PDI-T-EG**:**PBDTTT-C-T**/Ca/Al, the 1:1 blend of donor:acceptor material gave, after using 5% 1,8-diiodooctane (DIO) as cosolvent, a PCE of 4.03%, with V_{oc} of 0.85 V, J_{sc} of 8.86 mA cm^{-2} and FF of 0.541. On the other hand, **PDI-1**, under the same conditions, yielded devices with a very low PCE of 0.13%. Using AFM, it was demonstrated that the use of 5% DIO produced a more favorable phase separation in the blend. The electron and hole mobilities in the BHJ blended films were $\mu_e = 1.0 \times 10^{-3}$ cm^2 V^{-1} s^{-1} and $\mu_h = 3.0 \times 10^{-3}$ cm^2 V^{-1} s^{-1}, respectively.[13]
This previous efficiency was further improved combining the donor polymer **PBDTTT-C-T** with a slightly modified PDI dimer: **Bis-PDI-T-MO** (Figure 3). Through a combined control of surface D/A compositions, phase separation, and phase size by screening the DIO concentration, the electric performance of a cell device in an inverted structure ITO/ZnO/D:A/MoOx/Ag was fine-tuned and the best efficiency of 4.34% (with V_{oc} of 0.78 V, J_{sc} of 10.17 mA cm^{-2} and FF of 0.548) was obtained, using 2% DIO as cosolvent.[14]

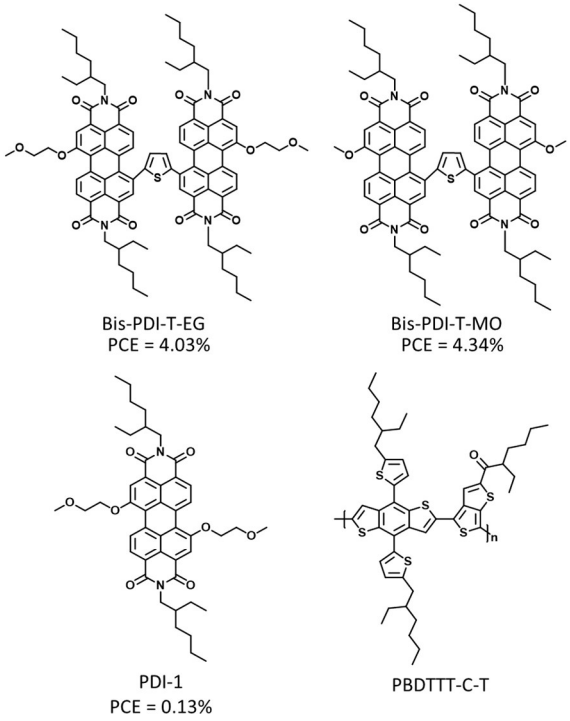

Fig. 3. Chemical structures of the PDI dimers **Bis-PDI-T-EG** and **Bis-PDI-T-MO**, PDI monomer **PDI-1** and the donor polymer **PBDTTT-C-T**.

In a step forward, a series of oligothiophene-bridged perylenediimide dimers (**PnTP**, n = 0-3) was synthesized (Figure 4). Density functional theory (DFT) calculations indicate that these molecules have a twisted structure due to the steric hindrance. **P0TP** exhibited a dihedral angle of 62.7º, while **P(1–3)TP** showed smaller dihedral angles of 50.7–52.3º. When **PnTP**s were blended with **PBDTTT-C-T**, the films showed hole mobilities from 10^{-6} to 10^{-5} cm^2 V^{-1} s^{-1} and electron mobilities from 10^{-6} to 10^{-4} cm^2 V^{-1} s^{-1}. Because **P0TP** exhibited the largest dihedral angle and steric hindrance among the four PDI dimers, which led to poor π–π stacking, the **PBDTTT-C-T**:**P0TP** blend showed the lowest electron mobility. On the other hand, oligothiophene-bridged PDI dimers possessed smaller dihedral angles and, consequently, **PBDTTT-C-T**:**P(1–3)TP** blend films exhibited higher electron mobilities.

Best performing OPVs [ITO/PEDOT:PSS/**PBDTTT-C-T**:**P(0–3)TP**/Ca/Al] were obtained by blending in a 1:1 ratio **PBDTTT-C-T** as the donor and **P(0–3)TP** as acceptors. Compared to **P0TP** (PCE: 0.76%), PDI dimers with the oligothiophene bridge gave better performance due to broader absorption and higher electron mobilities. The devices based on **PBDTTT-C-T**:**P1TP** with 3% DIO gave the best efficiency among these molecules: V_{oc} of 0.89 V, J_{sc} of 7.78 mA cm^{-2}, FF of 0.521 and PCE of 3.61%, due to the highest hole and electron mobilities of all the molecules. Increasing the number of thiophene units led to lower performances, which was attributed to lower hole and electron mobilities.

An AFM study of the film morphologies showed large aggregation domains (around 100 nm) and large phase separation in the **PBDTTT-C-T**:**P0TP** blend film, suggesting poor miscibility between the donor and acceptor. **PBDTTT-C-T**:**P2TP** and **PBDTTT-C-T**:**P3TP** blend films had smooth morphology and small aggregation domains (around 10 nm), indicating good donor-acceptor miscibility, which was beneficial to exciton diffusion/separation but not favorable for charge transport and finally led to low mobilities and low PCEs. In the **PBDTTT-C-T**:**P1TP** blend film, suitable aggregation domains (tens of nanometers) and phase separation facilitated both exciton diffusion/separation and charge transport, thus the **PBDTTT-C-T**:**P1TP** blend film exhibited the highest hole and electron mobilities and the best device performance.[15]

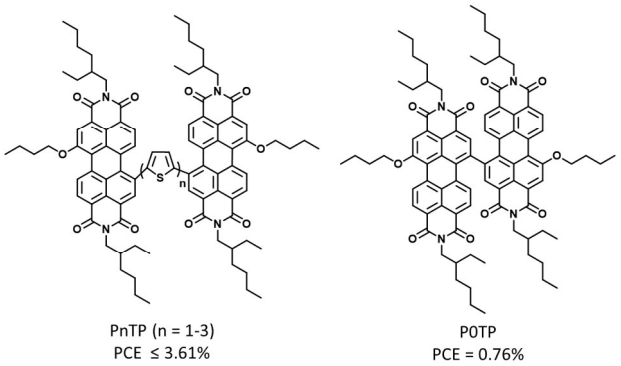

Fig. 4. Chemical structures of **PnTP** (n = 0-3).

The flexible or semiflexible geometries of the previous PDI dimers decrease the effective conjugation and raise the rotational disorder and the reorganization energy, negatively affecting to charge mobility and morphology in the OPV. On the other hand, a nonplanar geometry is required to ensure the formation of a bicontinuous network with donor materials. The combination of these two statements leads to an ideal PDI acceptor possessing enhanced conjugation and molecular packing order to assure charge mobility but keeping a nonplanar structure to avoid the formation of large aggregates. Following these thoughts, **FPDI-F**, **FPDI-T** and **FPDI-Se** were synthesized (Figure 5). All three compounds have similar energy levels, but different molecular geometries due to the different size of the chalcogen atom. Compared to the non-fused systems, these compounds have higher lying LUMOs (which is beneficial for a larger V_{oc}). OPVs were prepared in an inverted architecture ITO/ZnO/**PTB7-Th**:**FPDI**/MoO_3/Ag, where the optimal blending ratio donor polymer:**FPDI** was found to be 1:2. The best performance was obtained with **FPDI-T** (PCE = 5.76%, V_{oc} = 0.94 V, J_{sc} = 11.80 mA cm^{-2} and FF = 0.52), which was increased by using 1-chloronaphthalene (CN) as a solvent additive to modulate the morphology (PCE = 6.72%, V_{oc} = 0.94 V, J_{sc} = 12.48 mA cm^{-2} and FF = 0.58). Devices based on **FPDI-Se** showed slightly worse performances (PCEs of 4.65 and 5.77% in the absence and presence of CN, respectively), while those based on **FPDI-F** showed a modest 3.29%. The difference in PCE in this **FPDI** series was attributed to the different morphology. μ_e, being two orders of magnitude lower than μ_h, was the limiting factor of the device performance, especially for J_{sc} and FF.[16]

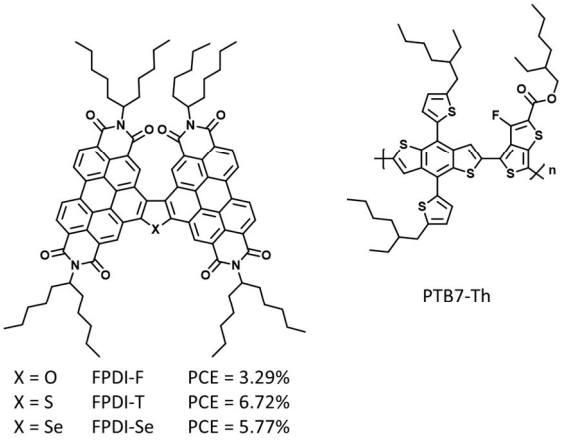

Fig. 5. Chemical structures of **FPDI-X** (X = O, S, Se).

2.2. Dimerization by direct linkage through the imide nitrogen

In 2012, the nonplanar dimeric **PDI-1** (Figure 6) was used in a fullerene-free OPV blended with the 2D-conjugated polymer **PBDTTT-C-T** (Figure 3) in an inverted device geometry of ITO/ZnO/polymer-acceptor/MoO_x/Ag achieving an encouraging PCE of 2.78% with an V_{oc} of 0.76 V, a J_{sc} of 9.5 mA cm^{-2} and a FF of 0.46. This result was attributed to the twisted N-N single bond, as the PDI subunits were oriented perpendicular to each other to minimize the electronic repulsion between the oxygen atoms, which significantly weakened the aggregation effect of acceptors, reduced the formation of intermolecular states and expedited charge separation at the interface (Figure 7).[17]

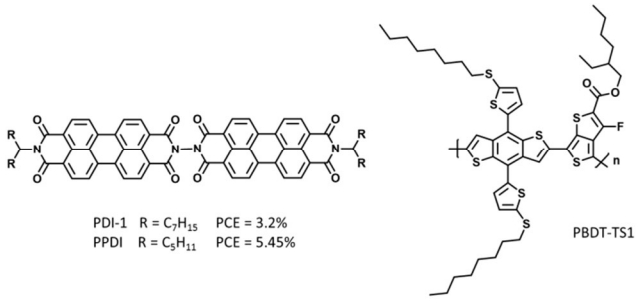

Fig 6. PDI dimers with a N-N linkage.

A more detailed study on this **PDI-1**:**PBDTTT-C-T** system (1:1 blend in the abovementioned inverted geometry) showed a maximum device efficiency of 3.2%, with V_{oc} of 0.77 V, a J_{sc} of 9.0 mA cm^{-2}, a FF of 0.46 and charge carrier mobilities μ_h = 2.74 × 10^{-4} cm^2 V^{-1} s^{-1} and μ_e = 1.47 × 10^{-4} cm^2 V^{-1} s^{-1} (μ_e/μ_h = 0.54).[18]

This study motivated the development of new strategies to produce dimeric PDIs with twisted structures. Thus, the dimer **PDI-1** was optimized by replacing the C_7H_{15} chains with C_5H_{11} ones. This modified acceptor, named as **PPDI** (Figure 6), was blended with **PBDTTT-C-T** in an OPV with ITO/PEDOT:PSS/**PBDTTT-C-T**:**PPDI**/Ca/Al architecture, yielding a PCE of 3.78% (V_{oc} of 0.76 ± 0.01 V, J_{sc} of 10.46 ± 0.26 mA cm^{-2} and FF of 0.49 ± 0.02).

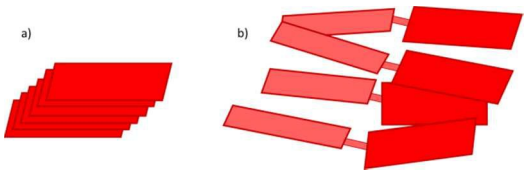

Fig. 7. a) Cristalline stacking of a planar PDI. b) Disrupted stacking of a twisted PDI-dimer.

Using the same device architecture but replacing the polymer donor by **PBDT-TS1** (Figure 6) in 1:1 ratio, the OPV gave an average PCE of 5.45% along with V_{oc} of 0.80 ± 0.01 V, J_{sc} of 12.85 ± 0.23 mA cm^{-2} and FF of 0.53 ± 0.02. The **PBDT-TS1**/**PPDI** device showed a relatively balanced hole/electron mobility (μ_e = 1.2 × 10^{-3} and μ_h = 8.9 × 10^{-3} cm^2 V^{-1} s^{-1}).

Also inverted OPVs, with a device geometry of ITO/PFN/polymer:acceptor/MoO_3/Al, were studied. The best-performing inverted devices based on **PBDT-TS1**/**PPDI** showed a PCE of 5.31% with a V_{oc} of 0.79 V, a J_{sc} of 13.19 mA cm^{-2} and a FF of 0.51.[19]

2.3. Dimerization by direct linkage through the bay positions

A study was performed comparing singly-linked, doubly-linked and triply-linked PDI dimers. The first one (**s-diPBI**) has a flexibly twisted structure with about 70º angle between the PDI moieties, while the second one (**d-diPBI**) possesses a locked twisted structure with nearly perpendicular PDI systems and the third one (**t-diPBI**) is rigid and almost planar (Figure 8). As expected, **t-diPBI** and **d-diPBI** showed much higher mobilities than **s-diPBI**. However, the best performing compound in solar cells with the structure ITO/PEDOT:PSS/**PBDTTT-C-T**:**diPBI**/Ca, was the *N*,*N*′-bis(pentylhexyl)-substituted **s-diPBI** with PCE of 3.63% (V_{oc} of 0.73 V, J_{sc} of 10.58 mA cm^{-2} and FF of 0.468), which was attributed to its flexibility and twisted structure that disrupts the crystallinity.[20]

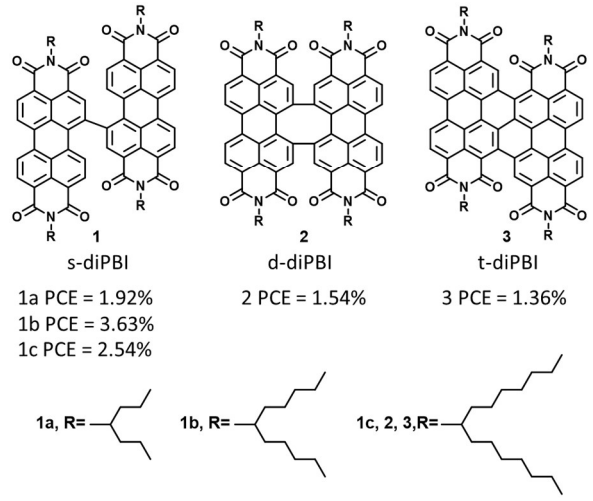

Fig. 8. PDI dimers linked through the bay positions.

The photovoltaic performances of **s-diPBI** were further enhanced by selecting as polymer counterpart **PBDTBDD** (Figure 9), due to its low-lying HOMO level and the strong aggregation effect in solution state. After selection of a ternary

processing solvent (o-dichlorobenzene:DIO:CN), a PCE of 4.39% (V_{oc} of 0.87 V, J_{sc} of 8.26 mA cm^{-2} and FF of 0.611) was realized in a conventional device architecture (ITO/PEDOT:PSS/**PBDTBDD**:**s-diPBI** 1:1/Ca/Al). This result was attributed to the high exciton dissociation efficiency, enhanced crystallinity as well as optimal phase separation.[21]

In a next report, still using **s-diPBI**, **PTB7-Th** (named in the paper as **PBDTT-F-TT**, Figure 9) was selected because of its deeper HOMO and red-shifted absorption. Also an inverted device architecture (ITO/ZnO/**PTB7-Th**:**s-diPBI**/MoO_3/Ag) was chosen because the results from optical modeling showed it offers better optical field distribution and exciton generation. In addition, the performance of the device was improved with a fullerene self-assembled monolayer (**PC$_{61}$BM**-SAM)-modified zinc oxide (ZnO) interlayer to enhance charge extraction. With all these modifications, a PCE of 5.90% (V_{oc} of 0.80 V, J_{sc} of 11.98 mA cm^{-2} and FF of 0.59) was reported. The estimated electron mobility was around 3.32×10^{-5} cm^2 V^{-1} s^{-1}, and hole mobility was 4.36×10^{-2} cm^2 V^{-1} s^{-1}. The shifted exciton generation profile towards the cathode in the inverted devices compensates for the poor electron mobility in the BHJ, which reduces charge recombination.[22]

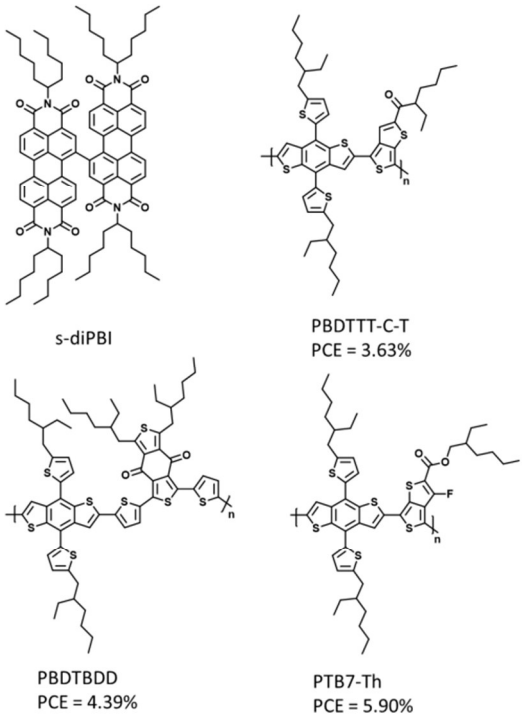

Fig. 9. Chemical structures of the acceptor **s-diPBI** and of the donor polymers **PBDTTT-C-T**, **PBDTBDD** and **PTB7-Th**.

A further improvement in this work line came with the synthesis of **SdiPBI-S** (Figure 10). Because of the rigidity increase introduced by the two fused thiophene rings, **SdiPBI-S** has a more twisted configuration. Thus, the dihedral angle between the two PDI subunits in **s-diPBI** is 67° and increases to 80° for **SdiPBI-S**. On the other hand, the electron-donating ability of the thiophene rings leads to a higher lying LUMO energy in comparison with **s-diPBI**, which is favorable for improving the V_{oc} of solar cells. Comparison of the UV-vis. spectra of **SdiPBI-S** in solution and in thin film shows similar optical absorption spectra in which the main absorption peaks are maintained at the same positions, indicative of weak aggregation in the solid state.

Conventional BHJ solar cells (ITO/PEDOT:PSS/**PDBT-T1**:**SdiPBI-S**/Ca/Al) based on **SdiPBI-S** and the wide-band-gap polymer **PDBT-T1** (Figure 10), 1:1 blend ratio with 0.75% of DIO, showed a PCE of 7.16% with an V_{oc} of 0.90 V, a J_{sc} of 11.98 mA cm^{-2} and a FF of 0.661.

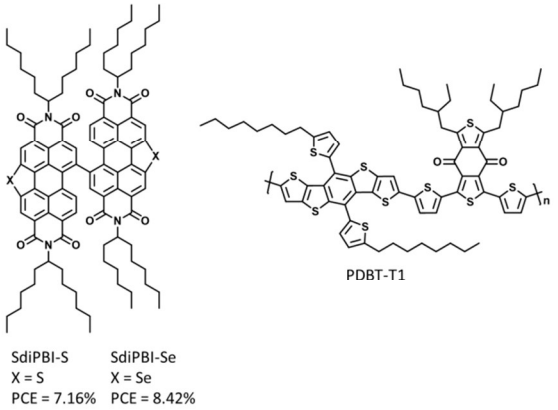

Fig. 10. Chemical structures of the acceptors **SdiPBI-S** and **SdiPBI-Se** and of the donor **PDBT-T1**.

For sake of comparison, solar cells based on the **PDBT-T1**/**s-diPBI** blend were fabricated in parallel. Under the same conditions, a PCE of 5.40% was obtained.

The high photovoltaic performance of **SdiPBI-S**-based cells was explained in terms of a favorable phase separation and balanced carrier mobilites in the BHJ films. The hole mobility was calculated to be $\mu_h = 1.2 \times 10^{-3}$ cm^2 V^{-1} s^{-1}, and the electron mobility was $\mu_e = 2.8 \times 10^{-3}$ cm^2 V^{-1} s^{-1} ($\mu_e/\mu_h = 2.3$). Finally, the DIO was found to increase the aggregation of the **SdiPBI-S** acceptor, leading to favorable phase separation and balanced carrier mobilites in the BHJ films.[10]

Taking into account that selenium has a bigger and more polarizable electron cloud than sulfur, which may enhance orbital overlap and charge carrier mobility, the next step was the study of **SdiPBI-Se** (Figure 10). The calculated geometry for this molecule showed a dihedral angle between the two PDI subunits of 77º, very close to that of **SdiPBI-S**, which ensured a weak aggregation in the solid state. OPVs with the device configuration ITO/PEDOT:PSS/**PDBT-T1**:**SdiPBI-Se**/Ca/Al, with a 1:1 weight ratio of donor and acceptor, showed a PCE of 7.55%, with J_{sc} = 11.75 mA cm^{-2}, V_{oc} = 0.95 V and FF = 0.678. The addition of 0.25% of DIO led to a record PCE of 8.42%, with J_{sc} = 12.49 mA cm^{-2}, V_{oc} = 0.96 V and FF = 0.702. Further increasing the amount of DIO lowered the PCE. The hole and the electron mobilities in the blend were found to be 3.6 10^{-3} and 4.8 10^{-3} cm^2 V^{-1} s^{-1}, respectively, pointing out to a nearly balanced charge transport ($\mu_e/\mu_h = 1.3$).[23]

A more elaborated approach was obtained by the covalent linking of two PDIs through an ethylene bridge. Because of its twisted molecular conformation, helical **hPDI2** (named in the paper as **Helical PDI 1**, Figure 11) does not aggregate strongly, while it keeps a relatively high electron mobility, good electron-accepting ability and a LUMO level (~4 eV) similar to those of **PC$_{61}$BM** and **PC$_{71}$BM**. OPVs were fabricated with this

material and the donor polymer **PTB7-Th** (named in the paper as **PBDTT-TT**) in an inverted geometry of ITO/ZnO/**PTB7-Th**:**hPDI2**/MoOx/Al. The best resulting **PTB7-Th**:**hPDI2** solar cell showed J_{sc} = 13.3 mA cm^{-2}, V_{oc} = 0.803 V, FF = 0.566 and PCE = 6.05%. These values are lower than those for the corresponding cells with fullerenes as the acceptors, but those partners were optimized for each other. For the **PTB7-Th**:**hPDI2** blend film, the hole and electron mobilities were calculated to be 2.9 × 10^{-4} and 3.4 × 10^{-4} cm^2 V^{-1} s^{-1}, respectively.

The authors showed that photogenerated excitons from **hPDI2** largely contribute to the photocurrent in these solar cells and conclude that electron and hole transfer from the photoexcited donor and acceptor, respectively, both occur efficiently at the donor−acceptor interfaces in the blended film.[24]

An extension of this synthetic methodology was achieved with the synthesis of oligomers **hPDI3** and **hPDI4** (Figure 11), the higher analogues of **hPDI2**, which consist of PDI subunits linked together by ethylene bridges. The steric congestion at the fusion point between the PDI units creates helical junctions, and longer oligomers form helical ribbons.

Electrochemical measurements reveal that the trimer **hPDI3** and the tetramer **hPDI4** can accept up to five electrons. The estimated LUMO energies for **hPDI3** and **hPDI4** are slightly lower than the LUMO level of PDI monomer and close to that of common n-type materials such as **PC$_{61}$BM**.

The electron mobility increases from dimer **hPDI2** to tetramer **hPDI4**, for the latter being 0.05 cm^2 V^{-1} s^{-1}. AFM studies show that compounds **hPDI2**−**hPDI4** formed very smooth films.[25]

The oligomers **hPDI3** and **hPDI4** were used with the polymer **PTB7-Th** (named in the article as **PBDTT-F-TT**) for the preparation of inverted solar cells (ITO/ZnO/**PTB7-Th**:**hPDI**/MoO_3/Al). This polymer was selected because its absorption bands are red shifted relative to those of **hPDI3** and **hPDI4**. For devices based on acceptor **hPDI3**, best results were obtained with donor: acceptor mass ratio of 1:1.5, using 1% DIO: PCE of 7.9%, with J_{sc} = 14.5 mA cm^{-2}, V_{oc} = 0.81 V and FF = 0.67. In the case of **hPDI4**, optimal device performance was achieved with donor-to-acceptor mass ratio of 1:1 and 1% DIO: PCE of 8.3%, with J_{sc} = 15.2 mA cm^{-2}, V_{oc} = 0.80 V and FF = 0.68. Transient absorption (TA) spectroscopy reveals that excitons generated in both the donor and acceptor phases contribute to the photocurrent by effective hole and electron transfer at the interface between donor and acceptor. For **PTB7-Th**:**hPDI3** blended film, the hole and electron mobilities were calculated to be 1.0 10^{-4} and 1.5 10^{-4} cm^2 V^{-1} s^{-1}, respectively, while for **PTB7-Th**:**hPDI4** blended film, the hole and electron mobilities were 1.2 10^{-4} and 1.5 10^{-5} cm^2 V^{-1} s^{-1}, respectively. The authors claimed that the film morphology of the active layer was composed of an interpenetrating network of **hPDI**-rich domains, embedded in **PTB7-Th**-rich matrix.[26]

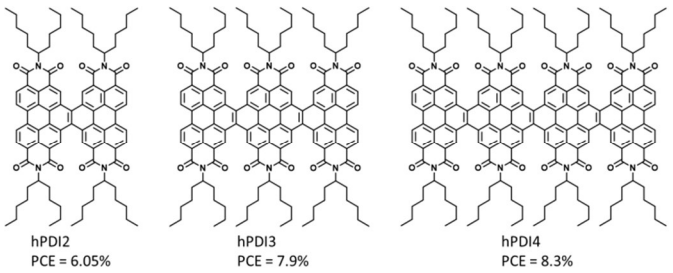

Fig. 11. Chemical structures of the acceptors **hPDI2**, **hPDI3** and **hPDI4**.

2.4. The quasi-spherical approach

Given that the most successful electron acceptor in OPVs, fullerene, has a ball-like structure, which allows isotropic charge transport, some research has been directed to the synthesis of a quasi-spherical PDI derivative, **Me-PDI$_4$** (Figure 12).

The geometry of **Me-PDI$_4$**, optimized using DFT calculations (B3LYP/6-31G*), shows that the PDIs are pointing to the vertices of a tetrahedron, with dihedral angles of 110.17º between each PDI unit and the connected phenyl group. This molecule has four degenerated LUMOs which can accept up to eight electrons.

A conventional structure of ITO/PEDOT:PSS/**PBDTTT-C-T**:**Me-PDI$_4$**/Ca/Al was firstly fabricated, which after addition of DIO and annealing showed a PCE of 2.35%. In order to further increase the device performance, an inverted device with a structure of ITO/ZnO/**PBDTTT-C-T**:**Me-PDI$_4$**/PEDOT:PSS/Ag was fabricated. With 3% DIO concentration and thermal annealing, the inverted device showed a PCE of 2.73%, with J_{sc} = 7.83 mA cm^{-2}, V_{oc} = 0.77 V and FF = 0.45.

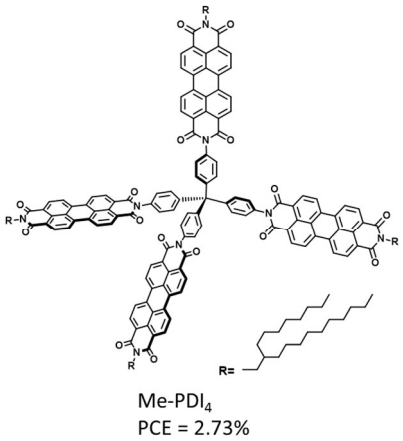

Fig. 12. Chemical structure of **Me-PDI$_4$**.

The as-prepared film under optimal conditions has a relatively low hole mobility of 5.55 10^{-5} cm^2 V^{-1} s^{-1} and a lower electron mobility of 1.78 10^{-6} cm^2 V^{-1} s^{-1}. Thus, the relatively low FF was attributed to the unbalanced electron–hole mobility (μ_e/μ_h = 0.032).[27]

Another step forward was achieved with the synthesis of **Tetra-PDI**, where the PDI subunits were attached to the tetraphenylsilane core through the bay positions (Figure 13). A

DFT calculation showed that, although each PDI unit and phenyl group in **Tetra-PDI** are covalently linked by rotatable single bonds, the four PDI units on the compact Si core have a 3D interlocked geometry, which is non-rotatable and differs from the previously reported nonplanar molecules. **Tetra-PDI** brings together four PDI units into a crowded space, thus enabling the energy transfer and electron communication among PDI units. Inverted devices (ITO/ZnO/**PTB7-Th**:**Tetra-PDI**/MoO_3/Ag) were fabricated to investigate the performance of solution-processed BHJ OPVs and after optimizing the blend ratio of the active layer to be 1:1.2 between **PTB7-Th** (named in the paper as **PBDTT-F-TT**, Figure 9) and **Tetra-PDI**, the device showed a PCE of 3.21% (with V_{oc} of 0.87 V, J_{sc} of 7.66 mA cm $^{-2}$ and FF of 0.48) without applying any post-treatments or additives. While DIO was found to have a negative effect on the performance of **Tetra-PDI** based devices, the addition of 3% CN led to an improved PCE of 3.54% (V_{oc} of 0.86 V, J_{sc} of 8.39 mA cm^{-2} and FF of 0.49).[28]

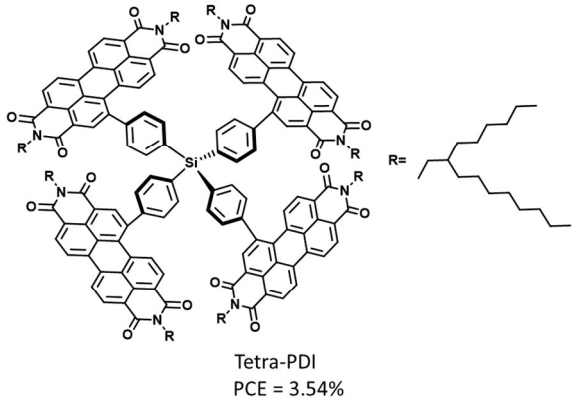

Fig. 13. Chemical structure of **Tetra-PDI**.

The same strategy as in the previous work led to the synthesis of compounds **TPC-PDI$_4$**, **TPSi-PDI$_4$** and **TPGe-PDI$_4$** (Figure 14), which have similar 3D structures except that the sizes of the core atoms (C, Si, and Ge) are different. Solar cell devices with a commonly used low bandgap donor polymer (**PffBT4T-2DT**, Figure 2) were fabricated (ITO/ZnO/**PffBT4T-2DT**:**TPX-PDI$_4$**/V_2O_5/Al, X = C, Si, Ge) showing PCEs of 4.3 % (V_{oc} = 0.96 V, J_{sc} = 9.2 mA cm^{-2} and FF = 0.49) for **TPC-PDI$_4$** and 4.2 % (V_{oc} = 0.94 V, J_{sc} = 8.5 mA cm^{-2} and FF = 0.53) for **TPSi-PDI$_4$** without any solvent additives or interlayers, indicating that these acceptors could be easily applied to fast and roll-to-roll industrial processing. Devices based on **TPGe-PDI$_4$** showed a PCE of 1.6 % due to stronger bimolecular recombination and monomolecular recombination in the **PffBT4T-2DT**/**TPGe–PDI$_4$** film than in the other films.[29]

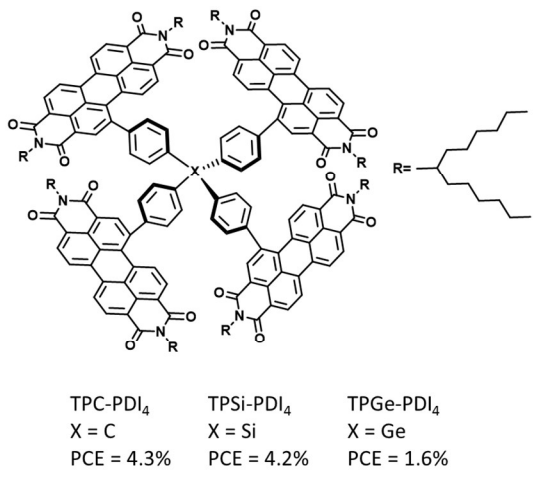

Fig. 14. Chemical structures of **TPX-PDI$_4$**.

A different approach to PDI-based three-dimensional structures has been achieved with the synthesis of **S(TPA-PDI)** (Figure 15), which takes advantage of the special propeller starburst molecular structure of TPA. The absorption of **S(TPA-PDI)** films suggests a weak intermolecular interaction and molecular aggregation in the film, because of the quasi-3D molecular structure of the molecule. The BHJ cells prepared using the low-bandgap polymer **PBDTTT-C-T** (Figure 3) as electron donor (ITO/PEDOT:PSS/**PBDTTT-C-T**:**S(TPA-PDI)**/Ca/Al) showed an efficiency of 3.32 % (V_{oc} = 0.88 V, J_{sc} = 11.92 mA cm^{-2} and FF = 0.336) when 5% DIO was used. The DIO solvent additive increased the film roughness and crystalline size. The crystalline domains were attributed to the self-organization of **PBDTTT-C-T**, which was beneficial to the ordered structure formation and charge transport in the thin film. The blend with the 5% DIO additive exhibited enhanced charge transport with a hole mobility of 7.17×10^{-4} cm^2 V^{-1} s^{-1} and electron mobility of 2.32×10^{-5} cm^2 V^{-1} s^{-1}.[30]

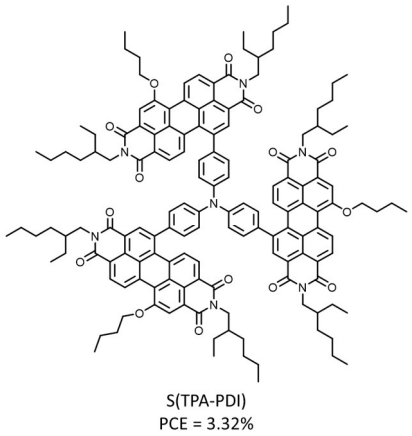

Fig. 15. Chemical structure of **S(TPA-PDI)**.

Another example of a 3D structure obtained from a highly twisted scaffold is represented by the tetraphenylethylene (TPE) core-based **TPE-PDI$_4$** (Figure 16). The TPE structure was selected because its four phenyl rings are highly twisted

due to strong steric hindrance: they all tilt by about 50° relative to the plane of the center double bond and form a "four-wing propeller-shape" molecular structure in the solid state. As a consequence, TPE-based molecules exhibit weak intermolecular interactions and thus, **TPE-PDI$_4$** shows excellent solubility in common organic solvents, and also forms ultra-smooth and amorphous films.

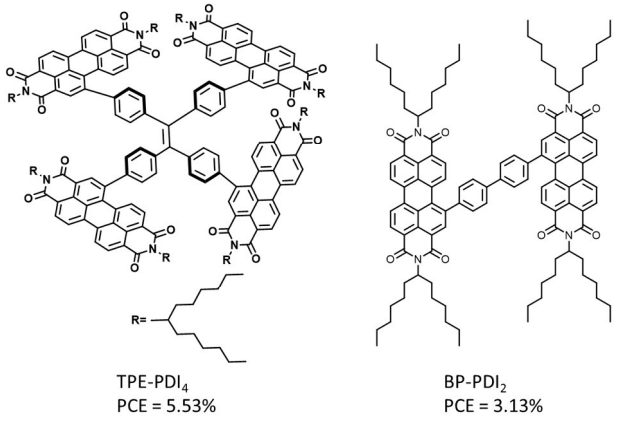

Fig. 16. Chemical structures of **TPE-PDI$_4$** and **BP-PDI$_2$**.

BHJ OPV devices were fabricated using **PTB7-Th** (named in the article as **PBDTT-F-TT**, Figure 9) as the donor and **TPE-PDI$_4$** as the acceptor. The authors claimed that without optimization of many of the device parameters, initial device-fabrication attempts yielded an impressive PCE of 5.53% (with J_{sc} = 11.7 mA cm^{-2}, V_{oc} = 0.91 V and FF = 0.52). This high performance, achieved without using any single or binary additives or special interlayers, may simplify device processing and optimization.

CV and UV–Vis data indicated the lack of conjugation between the four PDI units in **TPE-PDI$_4$**, which allows it to maintain a relatively high LUMO level and achieve OPVs with a higher V_{oc} than those of the corresponding PCBM-based cells. Moreover, the 3D structure of **TPE-PDI$_4$** facilitates the formation of a 3D charge-transport network and thus enables a reasonably good electron-transport ability. These advantageous features of **TPE-PDI$_4$** were clearly demonstrated by comparing **TPE-PDI$_4$** with **BP-PDI$_2$**, which has a 2D molecular structure.[31]

3. Modification of the film-forming kinetics

Shape is a remarkable difference between fullerenes and small-molecule acceptors, thus the spherical shape of the formers favours phase segregation giving rise to a nanoscale interpenetrating network, which accounts, in part, for the excellent performances of these solar cells. On the other hand, efficiencies in non-fullerene cells suffer by the lower electron mobility and recombination losses.

The twisted conformation of a PDI dimer such as **bis-PDI-T-EG** (Figure 3) is a hindrance to phase segregation in the blend and also to aggregation of the acceptor molecules.

Recently, a dramatic increase in the power conversion efficiency (from 1.4 up to 6.1%) in a polymer:small molecule (D:A) system of **PBDTTT-C-T** and **bis-PDI-T-EG** (Figure 3), has been described. This efficiency was achieved from a conventional single-junction solar cell with a structure of ITO/ PEDOT:PSS/donor:acceptor/Ca/Al, after using solvent-vapor annealing (SVA), a method to put the as-cast active film in the vapor of a solvent to reconstruct the film morphology. The improvement was attributed to the fine-tuning of the parameters relative to the film-forming kinetics, which was optimized by manipulation of the additive content during film processing, the volume of the host solvent for SVA, the volume ratio of the additive versus the host solvent for SVA, and the time for SVA. The result of this process was an increase in the photocurrent and the fill factor as a consequence of the reduction of the monomolecular and bimolecular loss and the improvement of the electron mobility. These improvements were associated with an enhancement of the phase segregation and consequently an enhancement of the self-aggregation of the donor and acceptor molecules in the solar cell blend.[32]

Table 1. Summary of the PV performances of PDIs in BHJ solar cells.

Acceptor	HOMO (eV)	LUMO (eV)	Donor	V_{oc} (V)	J_{sc} (mA/cm^2)	FF	PCE (%)	ref
PDI-1	-3.74	-5.81	P3HT	0.54	4.24	0.55	1.27[a]	11
PDI-2	-3.76	-5.86	P3HT	0.57	2.70	0.58	0.90[a]	11
PDI-3	-3.77	-5.68	P3HT	0.46	4.18	0.46	0.95[a]	11
PDI-4	-3.75	-5.54	P3HT	0.52	5.20	0.58	1.56[a]	11
PDI-5	-3.71	-5.71	P3HT	0.61	6.27	0.60	2.28[a]	11
PDI-6	-3.71	-5.71	P3HT	0.61	5.92	0.65	2.35[a]	11
PDI-6	-3.83	-5.90	PffBT4t-2DT	0.98	10.7	0.57	6.3[a]	12
Bis-PDI-T-EG	-3.84	-5.65	PBDTTT-C-T	0.85	8.86	0.541	4.03	13
Bis-PDI-T-EG	-3.84	-5.65	PBDTTT-C-T	0.84	12.83	0.564	6.08	32
Bis-PDI-T-MO	-3.84	-5.65	PBDTTT-C-T	0.78	10.17	0.548	4.34[a]	14
P0TP	-3.84	-5.74	PBDTTT-C-T	0.84	2.11	0.427	0.76	15
P1TP	-3.72	-5.66	PBDTTT-C-T	0.89	7.78	0.521	3.61	15
FPDI-F	-3.80	-6.01	PTB7-Th	0.92	8.71	0.40	3.29[a]	16
FPDI-T	-3.77	-5.98	PTB7-Th	0.94	12.48	0.58	6.72[a]	16
FPDI-Se	-3.76	-5.96	PTB7-Th	0.92	11.19	0.55	5.77[a]	16
PDI-1	-4.1	-5.9	PBDTTT-C-T	0.77	9.0	0.46	3.2[a]	18
PPDI	-3.49	-6.01	PBDTTT-C-T	0.76	10.46	0.49	3.78	19
PPDI	-3.49	-6.01	PBDT-TS1	0.80	12.85	0.53	5.45	19
PPDI	-3.49	-6.01	PBDT-TS1	0.79	13.19	0.51	5.31[a]	19
s-diPBI	-3.92	-5.9	PBDTTT-C-T	0.73	10.58	0.468	3.63	20
s-diPBI	-3.92	-5.9	PBDTBDD	0.87	8.26	0.611	4.39	21
s-diPBI	-3.92	-5.9	PTB7-Th	0.80	11.98	0.59	5.90[a]	22
SdiPDI-S	-3.85	[b]	PDBT-T1	0.90	11.98	0.661	7.16	10
SdiPBI-Se	-3.87	[b]	PDBT-T1	0.96	12.49	0.702	8.42	23
hPDI2	-3.77	-6.04	PTB7-Th	0.803	13.3	0.566	6.05[a]	24
hPDI3	-3.86	-6.23	PTB7-Th	0.81	14.5	0.67	7.9[a]	26
hPDI4	-3.91	-6.26	PTB7-Th	0.80	15.2	0.68	8.3[a]	26
Me-PDI$_4$	-3.82	-5.96	PBDTTT-C-T	0.77	6.47	0.472	2.35	27
Me-PDI$_4$	-3.82	-5.96	PBDTTT-C-T	0.77	7.83	0.450	2.73[a]	27
Tetra-PDI	-4.00	-5.97	PTB7-Th	0.86	8.25	0.48	3.54[a]	28
TPC-PDI$_4$	-3.75	-6.00	PffBT4T-2DT	0.96	9.2	0.49	4.3	29
TPSi-PDI$_4$	-3.75	-6.01	PffBT4T-2DT	0.94	8.5	0.53	4.2	29
TPGe-PDI$_4$	-3.68	-5.94	PffBT4T-2DT	0.92	5.0	0.37	1.6	29
S(TPA-PDI)	-3.70	-5.40	PBDTTT-C-T	0.88	11.92	0.336	3.32	30
TPE-PDI$_4$	-3.72	-5.77	PTB7-Th	0.91	11.7	0.52	5.53	31
BP-PDI$_2$	-3.72	-5.81	PTB7-Th	0.93	8.6	0.39	3.13	31

[a] Values were obtained from inverted devices. [b] Values not provided.

Summary and future perspectives

For the development of nonfullerene acceptors, researches on PDIs would possibly still be dominative in future. Selecting appropriate linkage units to get finely controlled aggregation and transporting properties seems to be the major research direction.[33]

We believe that this mini review provides an overview of the most recent progresses in this particular field and will serve as

guidance for strategies to design efficient perylenediimides for OPVs.

Acknowledgments

We thank financial support from Ministry of Economy and Competitiveness (Mineco) of Spain, Generalitat Valenciana and the European FEDER funds (CTQ2014-55798-R, CTQ2013-47922-R, Prometeo 2012/010, ACOMP2013/024, and ISIC/2012/008 Institute of Nanotechnologies for Clean Energies).

Affiliations

a - Universidad Miguel Hernández, Instituto de Bioingeniería, Avda. de la Universidad,s/n, Elche, Alicante, Spain. *E-mail: asastre@umh.es;
Fax: +34 966658351; Tel: +34 966658408

Notes and references

1 (a) Y. J. Cheng, S. H. Yang and C. S. Hsu, *Chem. Rev.*, 2009, **109**, 5868; (b) Y. Z. Lin, Y. F. Li and X. W. Zhan, *Chem. Soc. Rev.*, 2012, **41**, 4245.

2 (a) J. B. You, L. T. Dou, K. Yoshimura, T. Kato, K. Ohya, T. Moriarty, K. Emery, C. C. Chen, J. Gao, G. Li and Y. Yang, *Nat. Commun.*, 2013, **4**, 1446; (b) J.-D. Chen, C. Cui, Y.-Q. Li, L. Zhou, Q.-D. Ou, C. Li, Y. Li and J.-X. Tang, *Adv. Mater.*, 2015, **27**, 1035; (c) B. Kan, M. Li, Q. Zhang, F. Liu, X. Wan, Y. Wang, W. Ni, G. Long, X. Yang, H. Feng, Y. Zuo, M. Zhang, F. Huang, Y. Cao, T. P. Russell and Y. Chen, *J. Am. Chem. Soc.*, 2015, **137**, 3886.

3 (a) B. C. Thompson, J. M. J. Fréchet, *Angew. Chem., Int. Ed.*, 2008, **47**, 58; (b) L. Dou, J. You, Z. Hong, Z. Xu, G. Li, R. A. Street and Y. Yang, *Adv. Mater.*, 2013, **25**, 6642.

4 H. Li, Y.-J. Hwang, B. A. E. Courtright, F. N. Eberle, S. Subramaniyan and S. A. Jenekhe, *Adv. Mater.*, 2015, **27**, 3266.

5 Y. Zhong, M. T. Trinh, R. Chen, W. Wang, P. P. Khlyabich, B. Kumar, Q. Xu, C.-Y. Nam, M. Y. Sfeir, C. Black, M. L. Steigerwald, Y.-L. Loo, S. Xiao, F. Ng, X.-Y. Zhu and C. Nuckolls, *J. Am. Chem. Soc* 2014, **136,** 15215

6 C. B. Nielsen, S. Holliday, H.-Y. Chen, S. J. Cryer and I. McCulloch, Acc. Chem. Res., 2015, **48**, 2803.

7 (a) H. Langhals, *Heterocycles*, 1995, **40**, 477; (b) F. Würthner, *Chem. Commun.*, 2004, 1564; (c) H. Langhals, *Helv. Chim. Acta*, 2005, **88**, 1309.

8 (a) C. Huang, S. Barlow and S. R. Marder, *J. Org. Chem.* 2011, **76**, 2386; (b) C. Li and H. Wonneberger, *Adv. Mater.,* 2012, **24**, 613.

9 (a) T. L. Ye, R. Singh, H. J. Butt, G. Floudas and P. E. Keivanidis, *ACS Appl. Mater. Interfaces*, 2013, **5**, 11844; (b) R. Singh, E. Aluicio-Sarduy, Z. Kan, T. Ye, R. C. I. MacKenzie, and P. E. Keivanidis, *J. Mater. Chem. A*, 2014, **2**, 14348; (c) A. Sharenko, C. M. Proctor, T. S. van der Poll, Z. B. Henson, T. Q. Nguyen and G. C. Bazan, *Adv. Mater.*, 2013, **25**, 4403; (d) M. Guide, S. Pla, A. Sharenko, P. Zalar, F. Fernández-Lázaro, A. Sastre-Santos and T.-Q. Nguyen, *Phys. Chem. Chem. Phys.*, 2013, **15**, 18894 (e) A. Sharenko, D. Gehrig, F. Laquai and T. Q. Nguyen, *Chem. Mater.*, 2014, **26**, 4109.

10 D. Sun, D. Meng, Y. Cai, B. Fan, Y. Li, W. Jiang, L. Huo, Y. Sun and Z. Wang, *J. Am. Chem.Soc.*, 2015, **137**, 11156.

11 Q. Yan, Y. Zhou, Y.-Q. Zheng, J. Pei and D. Zhao, *Chem. Sci.*, 2013, **4**, 4389.

12 J. Zhao, Y. Li, H. Lin, Y. Liu, K. Jiang, C. Mu, T. Ma, J. Y. L. Lai, H. Hu, D. Yu and H. Yan, *Energy Environ. Sci.*, 2015, **8**, 520.

13 X. Zhang, Z. Lu, L. Ye, C. Zhan, J. Hou, S. Zhang, B. Jiang, Y. Zhao, J. Huang, S. Zhang, Y. Liu, Q. Shi, Y. Liu and J. Yao, *Adv.Mater.*, 2013, **25**, 5791.

14 Z. Lu, B. Jiang, X. Zhang, A. Tang, L. Chen, C. Zhan and J. Yao, *Chem. Mater.*, 2014, **26**, 2907.

15 J. Wang, Y. Yao, S. Dai, X. Zhang, W. Wang, Q. He, L. Han, Y. Lin and X. Zhan, *J. Mater. Chem. A,* 2015, **3**, 13000.

16 H. Zhong, C.-H. Wu, C.-Z. Li, J. Carpenter, C.-C. Chueh, J.-Y. Chen, H. Ade and A. K.-Y. Jen, *Adv. Mater.* 2016, **28**, 951.

17 R. R. Shivanna, S. K. Kandappa and K. S. Narayan, *J. Phys. Chem. Lett.*, 2012, **3**, 2405.

18 R. Shivanna, S. Shoaee, S. Dimitrov, S. K. Kandappa, S. Rajaram, J. R Durrant and K. S. Narayan, *Energy Environ. Sci.* 2014, **7**, 435.

19 L. Ye, K. Sun, W. Jiang, S. Zhang, W. Zhao, H. Yao, Z. Wang and J. Hou, *ACS Appl. Mater. Interfaces*, 2015, **7**, 9274.

20 W. Jiang, L. Ye, X. Li, C. Xiao, F. Tan, W. Zhao, J. Hou and Z. Wang, *Chem. Commun.*, 2014, **50**, 1024

21 L. Ye, W. Jiang, W. Zhao, S. Zhang, D. Qian, Z. Wang and J. Hou, *Small*, 2014, **10**, 4658.

22 Y. Zang, C.-Z. Li, C.-C. Chueh, S. T. Williams, W. Jiang, Z.-H. Wang, J.-S. Yu and A. K.-Y. Jen, *Adv. Mater.*, 2014, ***26***, 5708.

23 D. Meng, D. Sun, C. Zhong, T. Liu, B. Fan, L. Huo, Y. Li, W. Jiang, H. Choi, T. Kim, J. Y. Kim, Y. Sun, Z. Wang and A. J. Heeger, *J. Am. Chem. Soc.*, 2016, **138**, 375.

24 Y. Zhong, M. T. Trinh, R. Chen, W. Wang, P. P. Khlyabich, B. Kumar, Q. Xu, C.-Y. Nam, M. Y. Sfeir, C. Black, M. L. Steigerwald, Y.-L. Loo, S. Xiao, F. Ng, X.-Y. Zhu and C. Nuckolls, *J. Am. Chem. Soc.*, 2014, **136**, 15215.

25 Y. Zong, B. Kumar, S. Oh, M. T. Trinh, Y. Wu, K. Elbert, P. Li, X. Zhu, S. Xiao, F. Ng, M. L. Steigerwald and C. Nuckolls, *J. Am. Chem. Soc.*, 2014, **136**, 8122.

26 Y. Zhong, M. T. Trinh, R. Chen, G. E. Purdum, P. P. Khlyabich, M. Sezen, S. Oh, H. Zhu, B. Fowler, B. Zhang, W. Wang, C.-Y. Nam, M. Y. Sfeir, C. T. Black, M. L. Steigerwald, Y.-L. Loo, F. Ng, X.-Y. Zhu and C. Nuckolls, *Nature Commun.*, 2015, **6**, 8242.

27 W. Chen, X. Yang, G. Long, X. Wan, Y. Chen and Q. Zhang, *J. Mater. Chem. C*, 2015, **3**, 4698.

28 S.-Y. Liu, C.-H. Wu, C.-Z. Li, S.-Q. Liu, K.-H. Wei, H.-Z. Chen and A. K.-Y. Jen, *Adv. Sci.*, 2015, **2**, 1500014.

29 Y. Liu, J. Y. L. Lai, S. Chen, Y. Li, K. Jiang, J. Zhao, Z. Li, H. Hu, T. Ma, H. Lin, J. Liu, J. Zhang, F. Huang, D. Yu and H. Yan, *J. Mater. Chem. A*, 2015, **3**, 13632.

30 Y. Lin, Y. Wang, J. Wang, J. Hou, Y. Li, D. Zhu and X. Zhan, *Adv. Mater.*, 2014, **26**, 5137.

31 Y. Liu, C. Mu, K. Jiang, J. Zhao, Y. Li, L. Zhang, Z. Li, J. Y. L. Lai, H. Hu, T. Ma, R. Hu, D. Yu, X. Huang, B. Z. Tang and H. Yan, *Adv. Mater.*, 2015, **27**, 1015.

32 X. Zhang, C. Zhan and J. Yao, *Chem. Mater.*, 2015, **27**, 166.

33 H. Fan and X. Zhu, *Sci. China Chem.*, 2015, **58**, 922.

